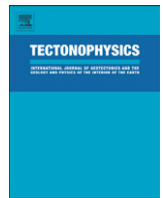




Contents lists available at ScienceDirect

Tectonophysics

journal homepage: www.elsevier.com/locate/tecto

Constraints on mantle viscosity structure from continental drift histories in spherical mantle convection models

T. Rolf^{a, b, *}, F.A. Capitanio^b, P.J. Tackley^c

^a Centre for Earth Evolution and Dynamics (CEED), University of Oslo, Norway

^b School of Earth, Atmosphere and Environment, Monash University, VIC 3800, Australia

^c Department of Earth Sciences, ETH Zurich, Switzerland

ARTICLE INFO

Article history:

Received 7 September 2016

Received in revised form 3 March 2017

Accepted 29 April 2017

Available online xxxxx

Keywords:

Continental drift
Mantle convection
Plate motions
Viscosity structure

ABSTRACT

Earth's continents drift in response to the force balance between mantle flow and plate tectonics and actively change the plate-mantle coupling. Thus, the patterns of continental drift provide relevant information on the coupled evolution of surface tectonics, mantle structure and dynamics. Here, we investigate rheological controls on such evolutions and use surface tectonic patterns to derive inferences on mantle viscosity structure on Earth. We employ global spherical models of mantle convection featuring self-consistently generated plate tectonics, which are used to compute time-evolving continental configurations for different mantle and lithosphere structures. Our results highlight the importance of the wavelength of mantle flow for continental configuration evolution. Too strong short-wavelength components complicate the aggregation of large continental clusters, while too stable very long wavelength flow tends to enforce compact supercontinent clustering without reasonable dispersal frequencies. Earth-like continental drift with episodic collisions and dispersals thus requires a viscosity structure that supports long-wavelength flow, but also allows for shorter-wavelength contributions. Such a criterion alone is a rather permissive constraint on internal structure, but it can be improved by considering continental-oceanic plate speed ratios and the toroidal-poloidal partitioning of plate motions. The best approximation of Earth's recent tectonic evolution is then achieved with an intermediate lithospheric yield stress and a viscosity structure in which oceanic plates are $\sim 10^3 \times$ more viscous than the characteristic upper mantle, which itself is $\sim 100\text{--}200 \times$ less viscous than the lowermost mantle. Such a structure causes continents to move on average $\sim (2.2 \pm 1.0) \times$ slower than oceanic plates, consistent with estimates from present-day and from plate reconstructions. This does not require a low viscosity asthenosphere globally extending below continental roots. However, this plate speed ratio may undergo strong fluctuations on timescales of several 100 Myr that may be linked to periods of enhanced continental collisions and are not yet captured by current tectonic reconstructions.

© 2017 Elsevier B.V. All rights reserved.

1. Introduction

Earth is a dynamic system in which surface tectonics and mantle dynamics operate together. For the present-day, the interplay of these components is constrained by a variety of geological and geophysical methods. However, back in deep time the available constraints become much looser, thus, our understanding of the structure and the dynamic evolution of the coupled plate-mantle system is vague.

Continents, in particular the cratons, resist recycling by plate tectonic processes even on geologically long timescales and thus provide our most comprehensive archive for Earth's tectonic history prior to the break-up of Pangea for which no oceanic seafloor is preserved. Continental drift is determined by the balance of forces generated from tectonics and mantle flow (e.g. Forsyth and Uyeda, 1975). However, continents themselves are an integral part of the plate-mantle system and affect the system's evolution. They confine the location of nascent subduction zones, which can explain the age distribution of Earth's seafloor (Coltice et al., 2012), and increase the wavelength of mantle flow (Tackley, 2000a; Phillips and Bunge, 2005; Grigné et al., 2007), an essential ingredient for the assembly of supercontinents (Zhang et al., 2009; Rolf et al., 2014). Such large continental clusters possibly cause large-scale subcontinental heat anomalies (e.g. Coltice et al., 2009; Brandl et al., 2013) and

* Corresponding author at: Centre for Earth Evolution and Dynamics, University of Oslo, Norway.

E-mail addresses: tobias.rolf@geo.uio.no (T. Rolf), fabio.capitanio@monash.edu (F. Capitanio), paul.tackley@erdw.ethz.ch (P. Tackley).

redistribution of subduction with implications for global mantle flow reorganisation (Zhong et al., 2007), the location of rising plumes underneath supercontinents (Heron et al., 2015) and possibly the evolution of deep thermochemical structures (McNamara and Zhong, 2005b; Bull et al., 2014; Trim and Lowman, 2016).

All these effects eventually impact the tectonic plates at the surface and their motion, the understanding of which, at present and throughout Earth’s evolution, is a fundamental goal of geodynamic research. Specifically, thick continental keels modify the coupling of surface plates and mantle flow (Zhong, 2001), particularly if they are not underlain by a weak asthenosphere (see e.g. van Summeren et al., 2012). This modifies the magnitude of shear tractions at the base of the lithosphere (Conrad and Lithgow-Bertelloni, 2006) and may ultimately impact the partitioning of slab-related plate motion driving forces, i.e. slab pull versus slab suction (Conrad and Lithgow-Bertelloni, 2002, 2004). The rheological contrast between continental and oceanic plates may moreover excite toroidal motion (Wen and Anderson, 1997; Becker, 2006), which is a substantial component of Earth’s surface motions (e.g. Lithgow-Bertelloni et al., 1993), but cannot be explained by simple density driven mantle flow (e.g. Bercovici et al., 2000).

Understanding the drift of continents and the evolution of their configuration thus provides important insight into the link between mantle dynamics and surface tectonics, such that collisions, break-ups and the clustering of Earth’s continents add relevant constraints on the plate-mantle system. Inferences on the paleogeography of continents mostly come from paleomagnetic samples, which constrain the geomagnetic latitude of a continent for the time when the sample’s magnetic signature was generated (see e.g. Domeier et al., 2012). In addition, peaks in zircon age distributions (e.g. Pearson et al., 2007) may reveal periods of more frequent continental collisions (Condie and Aster, 2010) and provide some spatiotemporal information, even for the Precambrian. In such distributions, however, it is difficult to distinguish between signals caused by enhanced production (linked to more frequent collisions) or just preservation of crust. Moreover, the quality and spatial frequency of zircon samples is quite heterogeneous; in fact, the available data coverage becomes fragmentary for pre-Mesozoic times.

In contrast, numerical models of mantle convection (e.g. Gurnis, 1988; Lowman and Gable, 1999; Lenardic et al., 2003; Phillips and Bunge, 2005; Zhong et al., 2007) are capable of revealing the feedback between continents, plates, and interior dynamics through space and time. Only recently, however, have such models reached a stage in which these components of the plate-mantle system are linked fully consistently in a time-dependent geodynamic framework (Yoshida, 2013; Yoshida and Santosh, 2014; Yoshida and Hamano, 2015; Rolf et al., 2012; Rolf et al., 2014).

Using such a model, we elaborate on the idea to use the evolution of continental configuration as a constraint for models of Earth’s mantle, in particular their viscosity profile. Since the tectonic forces governing the feedback of continents, plates, and mantle flow depend on viscosities, our strategy here is to vary parameters determining viscosity structure, to analyse its effects on continental evolution and surface plate characteristics, and to infer an appropriate structure for approximating Earth-like tectonics based on this.

2. Method

Numerical solutions of mantle convection with self-consistently generated plate-like behaviour and continental drift obtained with the code StagYY (Tackley, 2008) are used to investigate the interplay between continental drift and mantle-lithosphere rheology. The model is an advancement of previous versions, which are described in more detail elsewhere (Rolf et al., 2012, 2014). The model reproduces the evolution of thermochemical mantle convection in a

Table 1

List of reference parameters used to convert non-dimensional model parameters and results into dimensional units (see Appendix A).

Symbol	Definition	Value
α_0	Thermal expansivity	$3 \times 10^{-5} \text{K}^{-1}$
g_0	Gravitational acceleration	10ms^{-2}
D_0	Mantle thickness	$2.89 \times 10^6 \text{m}$
ΔT	Temperature drop	2500K
T_S	Surface temperature	300K
ρ_0	Normal mantle density	3300kgm^{-3}
k_0	Thermal conductivity	$3.15 \text{Wm}^{-1} \text{K}^{-1}$
κ_0	Thermal diffusivity	$1 \times 10^{-6} \text{m}^2 \text{s}^{-1}$
η_0	Viscosity (at $T = \Delta T$)	$1 \times 10^{22} \text{Pas}$
T_E	Mantle transit time (Earth)	$6.3 \times 10^7 \text{yr}$

spherical shell with inner radius $R_C = 3480 \text{ km}$ and outer radius $R_S = 6370 \text{ km}$. While the deeper mantle has uniform composition, the lithosphere is compositionally heterogeneous due to the presence of continents. Model continents consist of a strong interior ($k = 1$, representing Archean craton) surrounded by weaker mobile rims ($k = 2$) (Lenardic et al., 2003). These different units are parametrised by two distinct compositional fields C_k , which continuously vary between 0 (no material of kind k) and 1 (only material of kind k present). To model the evolution of the fields C_k tracer particles are used to track the different compositions through time via the tracer-ratio method (Tackley and King, 2003). The different compositions are characterised by contrasts in density and rheological properties relative to the reference mantle ($C_1 = C_2 = 0$). The density contrast is specified by the buoyancy ratio $R_k = \Delta\rho_k / \rho_0 \alpha_0 \Delta T$, that is, the ratio of the compositional density difference $\Delta\rho_k$ to the thermal density variation $\rho_0 \alpha_0 \Delta T$. Here, $R_k = -0.4$ for both cratonic interiors and mobile rims, thus, $\Delta\rho_k \sim -100 \text{kgm}^{-3}$ using the parameters in Table 1.

In terms of rheology, continents have distinct contrasts in viscosity and yield stress (the maximum stress material can sustain before deforming plastically). The former is defined by the viscosity ratio $\Delta\eta_{C_k}$ of material k and the reference material at given temperature and depth. The latter is defined accordingly via the yield stress ratio $\Delta\sigma_{Y_k}$ (see Rolf et al., 2014). The effective temperature (T), depth (d), composition (C), and strain-rate ($\dot{\epsilon}$) dependent viscosity η is given by

$$\eta_T = \eta_d \cdot \exp \left[\frac{E_A}{T+1} - \frac{E_A}{2} \right] \prod_{k=1}^2 \exp [\ln(\Delta\eta_{C_k}) C_k], \tag{1}$$

$$\eta_Y = \frac{\sigma_Y}{2\dot{\epsilon}}, \sigma_Y = (\sigma_0 + d \sigma'_Y) \prod_{k=1}^2 \exp [\ln(\Delta\sigma_{Y_k}) C_k], \tag{2}$$

and $\eta = (1/\eta_T + 1/\eta_Y)^{-1}$. Here, E_A is the activation energy and the last term in Eq. (1) describes the dependence on composition as introduced above. In order to ensure craton longevity we chose $\Delta\eta_{C_1} = 100$ and $\Delta\eta_{C_2} = 0.1$ (following Yoshida, 2012), however, such choices depend on absolute viscosities, the details of the rheological laws and the timescales of interest (e.g. Doin et al., 1997; Lenardic and Moresi, 1999; Lenardic et al., 2003). η_d describes the depth-dependence, characterised by a viscosity jump $\Delta\eta_R$ at 660 km depth. Here, $1 \leq \Delta\eta_R \leq 100$ is variable (while it was fixed at $\Delta\eta_R = 1$ in Rolf et al., 2012, 2014). However, in order to keep the globally averaged viscosity unchanged, the condition $\int_{R_C}^{R_S} \eta_d dV = 1$ is enforced. In Eq. (2), η_Y describes the strain rate-dependent part ($\dot{\epsilon}$ is the 2nd invariant of the strain rate tensor), which is used to parametrise plastic yielding in the model. Yielding occurs if the material’s yield stress (σ_Y) is reached, which is composed of a constant (σ_0) and a depth-dependent part (σ'_Y). After inspection of flow solutions and exclusion of cases with significant plastic yielding at sublithospheric depth and by employing the plate diagnostics defined in Tackley (2000b),

$\sigma'_y = 1.2 \times 10^6$ ($\approx 1.5 \text{ MPa km}^{-1}$) was found to be an appropriate value for simulating plate-like behaviour. The surface value is a parameter varied here: $3.3 \times 10^4 \leq \sigma_0 \leq 6.6 \times 10^4$ ($\approx 120\text{--}240 \text{ MPa}$). These numbers concern ductile deformation; for brittle deformation, which dominates in Earth's crust, the surface value (cohesion) may be much smaller and the gradient (friction coefficient) much larger. We do not consider this here because the thin crustal layer is omitted in our model. The yield stress ratios are $\Delta\sigma_{y_1} = \Delta\sigma_{y_2} = 10$ in order to ensure craton longevity (Lenardic et al., 2003; Rolf et al., 2014).

The final ingredient to generate Earth-like tectonic behaviour is a parametrised asthenosphere in which viscosity is reduced by a factor $\Delta\eta_{AS} = 0.1$ where the solidus is exceeded (Tackley, 2000c). Here, the solidus increases with depth according to a fit to experimental data (see Xie and Tackley, 2004, and references therein). We did not vary $\Delta\eta_{AS}$ here because its actual value may not have first-order impact on the global plate-mantle coupling (e.g. Conrad and Lithgow-Bertelloni, 2006). Finally, we note that viscosity variation is generally limited to the interval $[10^{-4}, 10^7]\eta_0$.

2.1. Computed evolutions

We compute nine evolutions (M1–M9) that differ in the choice of E_A , $\Delta\eta_R$, and σ_0 (Table 2). Solutions are obtained by solving the governing equations on a YinYang grid with resolution $128 \times 384 \times 64$ for each of the 2 grid blocks. The grid is radially refined close to the top and bottom boundaries, which are both free-slip (see Tackley, 2008, for further details on the numerical solution strategy). The grid is randomly filled with 1.92×10^8 tracer particles to track compositions.

Rolf et al. (2014) studied purely internally heated cases, but here we consider heating from inside and from below. The applied internal heating rate is $H = 37.3$ ($\approx 3 \times 10^{-11} \text{ Wkg}^{-1}$) and the surface and basal temperature are T_S and $T_S + \Delta T$, respectively. The rather high H value is chosen in favour of a mantle predominantly heated from internal sources, which constitute 85–90% of the total heat budget. We do not consider evolution of H with time here, because our intention is to analyse the dynamics of modern-style tectonics rather than its evolution from a hotter Archean environment.

The applied Rayleigh number is $Ra_0 = \alpha_0 g_0 \Delta T D^3 \rho_0 / \kappa_0 \eta_0 \sim 6 \times 10^6$, where the reference viscosity η_0 is the volume-averaged viscosity at $T = \Delta T$. This may effectively reduce convective vigour and lead to somewhat higher viscosities than suggested for Earth. However, higher Ra_0 requires finer numerical resolution and causes much higher computational costs. Even so, the viscosity profiles here (see below) already seem much more Earth-like than in the related previous studies (Rolf et al., 2012, 2014).

Rolf et al. (2014) used a continent configuration with $N_C = 2$ continents, while here we use $N_C = 6$. With $N_C > 2$, continental configuration becomes non-trivial since fully assembled and dispersed states are merely end-members and hybrid configurations as observed on Earth are likely. We prescribe an initial configuration in which all continents are separated. We chose a continental thickness of $d_C = 0.083 \approx 240 \text{ km}$ in order to obtain thicker continental than oceanic lithosphere, which is important for the coupling between mantle flow and plates (Zhong, 2001; Conrad and Lithgow-Bertelloni, 2006). Each continent has a distinct polygonal shape, such that no symmetry is enforced. In total, continents initially cover $\sim 31\%$, which varies slightly with time as parts of their weak rims may be eroded. Our model is not yet capable of producing new continental material from dynamic processes.

By initially precluding advection of tracers in the flow, continental configuration is kept fixed in position until a statistically steady state is reached. Then afterwards, tracers and continental configuration evolve self-consistently in accordance to the computed flow fields for $\geq 2 \text{ Gyr}$. The chosen initial configuration imposes some geometric constraints on the flow, which disappear once continents drift and

their configuration becomes self-organised. In order to account for this, we ignore the first $\sim 500 \text{ Myr}$ of evolution in all time averages presented below.

2.2. Diagnostics

We discuss continental drift in terms of its rate v_C (averaged over all continents), its temporal fluctuation and its relation to the velocity v_0 of the remaining oceanic plates, $R_{OC}(t) = v_0(t)/v_C(t)$. All velocities discussed here are rms-velocities. These exclude net rotation since the vector of mean surface motion is subtracted from the velocity solution after each time step. This correction is employed only at the surface, such that deeper layers may include a net rotation component (cf. Becker, 2006). Following Tackley (2000b), we also analyse the partitioning of surface motions into toroidal and poloidal components, $R_{TP} = \sqrt{v_T^2/v_P^2}$.

In addition, we analyse continental configuration in terms of the number of assembled continent pairs $P_A(t)$. For simplicity, we only differentiate between two end-members (two blocks are either assembled or not) and do not estimate the distance over which two continental margins are connected, such that P_A has only integral values. For example, $P_A = 0$ means that all continents are separated from each other, while $P_A = N_C - 1 = 5$ if all continents form a chain, the minimum required for a supercontinent configuration (i.e. all six continents are assembled). $P_A > N_C - 1$ is possible for more compact assemblies (see e.g. Fig. 1b). However, $P_A = N_C - 1$ does not strictly imply that all continents are connected (e.g. when all continents except one form a compact cluster and the remaining one is separated). Because of that and because the continental polygons do not have a simple shape, their configurations were analysed based on visualisation of the flow solutions. Despite its limitations, we found P_A to be a useful measure for continental configuration evolution.

3. Results

3.1. Characteristic dynamics and plate-like behaviour

With internal heating as the main heat source, the dynamics of the surface boundary layer, in particular subduction and slab sinking, dominate the evolution. While modelled subduction at continental margins is single-sided, intraoceanic subduction is generally too symmetric compared to Earth (Fig. 1), a common problem in mantle flow computations with free-slip boundaries in which realistic bending of subducting plates is complicated (Cramer et al., 2012). Most intraoceanic slabs thus sink rather vertically into the mantle, but once they hit the upper-lower mantle boundary the applied viscosity contrast hinders their sinking, they deform and sink deeper slowly with various angles (Fig. 1).

Besides this simplified representation of subduction, most of the evolutions presented here feature plate-like behaviour in terms of surface mobility (plate velocities are typically $\sim 1.5\text{--}2\times$ the global average) and the localisation of deformation into narrow plate boundaries. The latter is revealed by the flatness proxy P_L (defined in Tackley, 2000b), which is generally > 0.8 , except for case M4, and possibly M3 (Fig. 2a). However, some remaining deformation is observed away from the plate boundaries (see e.g. Eastern hemisphere in Fig. 1b2). With the employed rheology, a typical viscosity contrast of $\sim 10^2$ may develop between plate interiors and margins (Fig. 2b). The most localised deformation, $P_L > 0.9$, is observed when this contrast tends to be highest, i.e. in cases with highest yield strength σ_0 (M7, M9). In specific scenarios during the evolutions though, the rheological contrast may be lower and plates and margins may not fully decouple, which possibly leads to some deformation in the plate interiors. However, diffuse deformation is also observed on Earth and may involve a significant portion of the oceanic lithosphere (e.g. Gordon, 1998). Finally, we note that the

Table 2
List of calculations and their characterising parameters, $\Delta\eta_R$, E_A , and σ_0 , as well as the diagnostics v_C , R_{OC} , R_{TP} , P_L , and P_A (see text for definitions). Case M8* is the reference case used for scaling. Case M8nc is identical to M8, but does not feature continents. E_A and σ_0 are given in kJ mol^{-1} and MPa, respectively (after applying the scaling described in Appendix A). The applied viscosity law implies rather high dimensional values of E_A ; however, they translate to thermal viscosity variations of 10^5 , 10^7 , and 10^9 , respectively.

Case	E_A	$\Delta\eta_R$	σ_0	$\langle v_C \rangle$	$\langle R_{OC} \rangle$	$\langle R_{TP} \rangle$	$\langle P_L \rangle$	$\langle P_A \rangle$
M1	670	1	120	1.2 ± 0.3	3.6 ± 1.1	0.60 ± 0.05	0.83 ± 0.02	3.3 ± 0.7
M2	670	30	120	2.2 ± 0.7	2.2 ± 0.6	0.50 ± 0.05	0.81 ± 0.02	3.2 ± 0.7
M3	670	100	120	3.6 ± 1.2	2.0 ± 0.4	0.45 ± 0.04	0.79 ± 0.03	4.8 ± 1.2
M4	480	30	120	2.5 ± 0.7	2.0 ± 0.6	0.41 ± 0.03	0.67 ± 0.02	1.6 ± 1.0
M5	860	30	120	1.6 ± 0.5	3.2 ± 1.5	0.64 ± 0.05	0.84 ± 0.02	4.3 ± 1.3
M6	670	100	180	3.5 ± 1.6	2.6 ± 1.6	0.51 ± 0.08	0.89 ± 0.02	4.4 ± 0.9
M7	670	100	240	3.6 ± 2.4	3.1 ± 2.2	0.47 ± 0.06	0.92 ± 0.02	6.6 ± 1.4
M8*	670	30	180	2.9 ± 1.2	2.2 ± 1.0	0.51 ± 0.07	0.88 ± 0.01	4.3 ± 1.7
M8nc	670	30	180	–	–	0.46 ± 0.03	0.80 ± 0.01	–
M9	670	30	240	2.3 ± 1.2	3.0 ± 1.3	0.58 ± 0.10	0.92 ± 0.02	4.6 ± 1.8

presence of strong continents seems to increase P_L (compare cases M8 and M8nc), probably because deformation is very limited in the surface area covered by them.

3.2. Reference tectonic evolution

We define a reference case (M8) to describe the long-term evolution observed in our models. In this case, the network of modelled plates is fairly heterogeneous, i.e. the surface is fragmented

into larger and smaller plates as observed on Earth (e.g. Bird, 2003; Mallard et al., 2016). This surface topology is time-dependent and old plate boundaries propagate or vanish, while new ones initiate elsewhere. Within 200 Myr, the global network of oceanic plates and plate boundaries has completely reorganised (compare panels a and b in Fig. 1).

This evolution further indicates that convergent plate boundaries are not predominantly confined to continent-ocean boundaries. This is the case despite the presence of weaker continental rims,

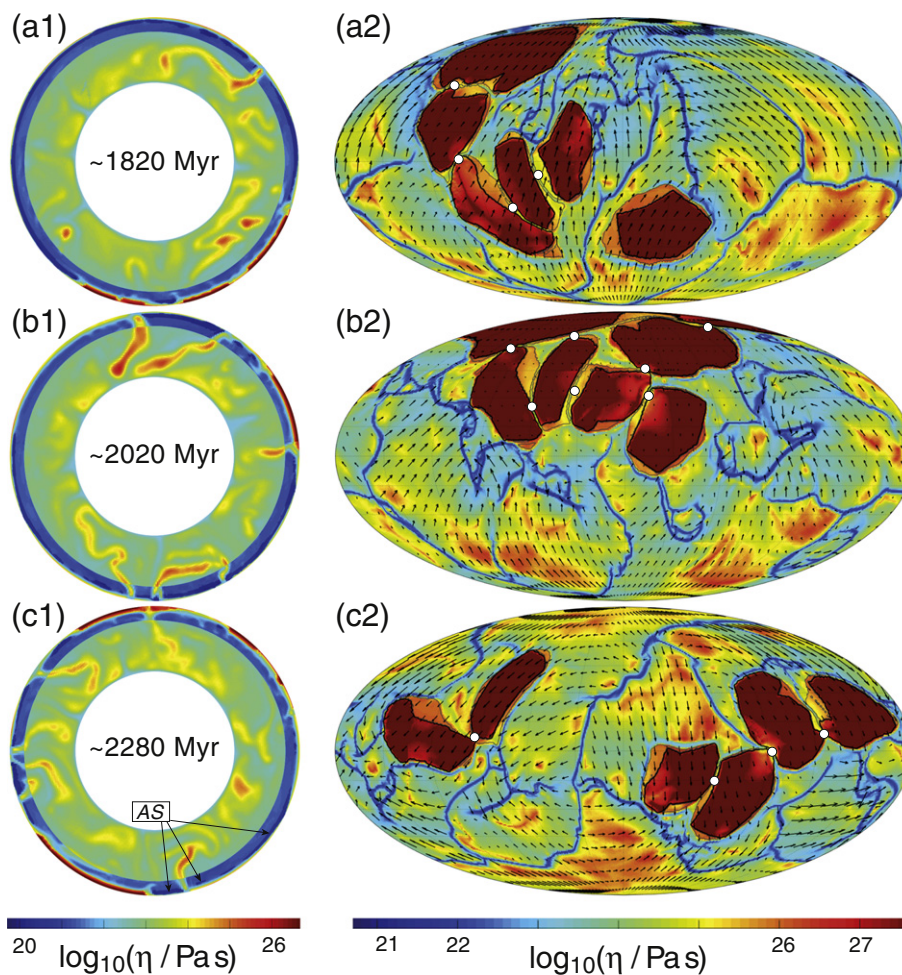


Fig. 1. Reference evolution M8. Panels (a)–(c) show 3 different times. Shown are equatorial cross-sections (left) and Mollweide projections (right). In the cross-sections, the low-viscosity asthenosphere (AS) is indicated by dark-blue patches, as highlighted for a few examples in (c). In the Mollweide projections, black arrows denote surface velocities. Cratons are contoured by black lines. Each white dot indicates an assembled continent pair that goes into the count of P_A (see text). (For interpretation of the references to colour in this figure legend, the reader is referred to the web version of this article.)

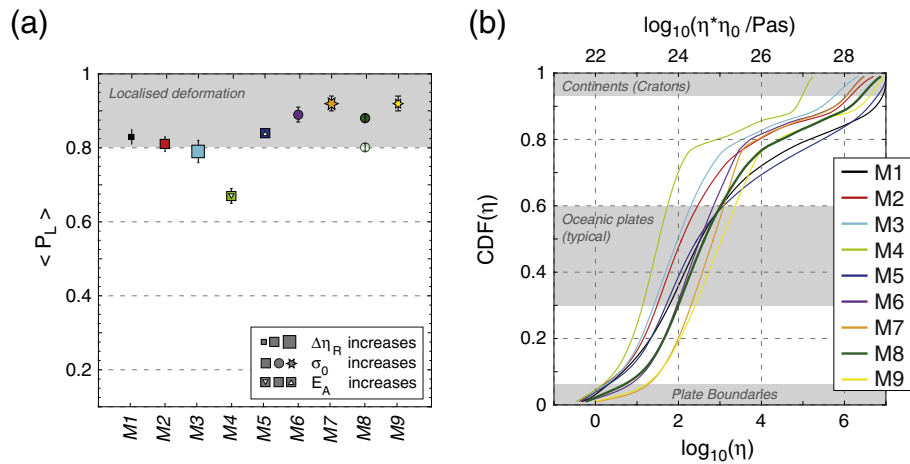


Fig. 2. Plate diagnostics for the presented cases. (a) Time-averaged plateness $\langle P_L \rangle$ (see Tackley, 2000b): $P_L \rightarrow 1$ indicates maximum localisation of deformation into narrow zones. Shown are mean values, error bars denote standard deviations. The empty circle denotes case M8nc without continents. (b) Time-averaged cumulative distribution function (CDF) of surface viscosity (η). This highlights the strength of lateral variations across the surface. Shaded areas indicate which range is typically observed for plate boundaries, oceanic plates and cratons, respectively.

at least for our chosen values for $\Delta\eta_{C2}$ and $\Delta\sigma_{Y2}$. However, the relation between continent and subduction location is rather time-dependent. Continents are usually driven towards zones of convergence, but once they reach such zones, subduction can fade (e.g. following continental collision) or can be maintained for some time. Thus, the continents change their configuration in accordance with the surrounding tectonics and mantle flow. In the reference case, this includes the assembly of continental clusters (possibly supercontinents) and their dispersion on a time scale of several 100 Myr.

A more quantitative picture of the tectonic evolution is provided by the ~ 2.5 Gyr time series of surface velocities, the ratio of oceanic and continental plate speeds, their poloidal-toroidal partitioning, and the degree of continental assembly (Fig. 3). First, an average continental plate always moves slower than an average oceanic plate (as noted by Forsyth and Uyeda (1975) for present-day Earth). In this case, variations in continental drift speed seem very cyclic with a rather well-defined period of ~ 400 Myr, in contrast to the oceanic plates, which usually experience fluctuations on shorter timescales of ~ 10 s of Myrs (Fig. 3a).

Consequently, the plate speed ratio R_{OC} is not characterised by a simple mean, but features strong fluctuations on timescales of several 100 Myr. Phases exist during which the continents move almost as fast as oceanic plates; on the other hand, the partitioning can be very strong ($R_{OC} > 5$) in phases in between. The partitioning is mostly governed by the speed of continents, which fluctuates much more than the average oceanic plate speed (maximum-minimum ratio of ~ 12 , respectively, ~ 3).

Throughout the entire evolution, surface motions contain a substantial toroidal component that is ~ 40 – 60% of the poloidal component ($\langle R_{TP} \rangle = 0.51 \pm 0.07$) (Fig. 3c). The strong continents induce significant lateral viscosity variations, which generally excite toroidal motion (see e.g. Bercovici et al., 2000). Recomputing the same evolution without continents (case M8nc) indeed indicates a small reduction in R_{TP} ($\sim 10\%$, see Table 2), but substantial toroidal motion is also present without continents (as in van Heck and Tackley, 2008). In both cases it also persists at greater depth, especially in the upper mantle, where lateral viscosity variations remain very strong (see Fig. 1). Some of the large amplitude fluctuations in R_{TP} seem to be linked to variations in R_{OC} and thus to the reorganisation of continental configuration. However, R_{TP} also experiences shorter-term variations more similar to the evolution of oceanic plate speeds.

Finally, we investigate the relation between variations in continental drift speed and supercontinent formation and subsequent dispersal by analysing the evolution of continental configuration via the proxy P_A (Fig. 3d). However, no direct relationship between slow continental drift (thus, high R_{OC}) and the presence of a supercontinent is given (if we define a supercontinent as any assembly of all six cratons). In fact, the evolution features only two supercontinents with lifetimes of ~ 350 and ~ 150 Myr, respectively. During these periods, R_{OC} is maximum, but maxima also occur when P_A is comparably low (e.g. at ~ 700 Myr, Fig. 3b/d). Nevertheless, some correlation seems to exist relating maxima in R_{OC} to foregoing increases in P_A (i.e. one or more collisions), because most of the kinetic energy of the colliding blocks may be consumed by deformation. On the other hand, minima in R_{OC} may be related to foregoing decreases in P_A (some continents separate) and continents will thus drift faster on average in less compact configurations, because then the chance to be drawn towards a major plate convergence zone is higher.

3.3. Rheological controls on surface motions

The rheology of the mantle and lithosphere and its lateral variations modulate oceanic-continental speed partitioning (Phillips and Bunge, 2005), the toroidal-poloidal decomposition of surface motions (Wen and Anderson, 1997; Zhong, 2001; Becker, 2006), the wavelength of convection (Bunge et al., 1996; Tackley, 1996; McNamara and Zhong, 2005a; Yoshida, 2008) and the timescales of continental assembly and dispersal (Zhang et al., 2009; Rolf et al., 2014). We thus illustrate how these properties affect the reference model presented above.

To do so, we vary the parameters $\Delta\eta_R$, E_A and σ_0 (Table 2) as introduced above. This leads to a range of different viscosity profiles that are similar in the bottom-most ~ 200 km, but vary by an order of magnitude in the lower mantle and by up to two orders of magnitude in the upper mantle, the lithosphere, and in the relative contrast between these layers (Fig. 4a).

The different viscosity profiles generate different mantle flow velocities (Fig. 4b). While absolute velocities are affected by the applied scaling to Earth (see Appendix A), average surface velocities vary by a factor of ~ 2 (corresponding to ~ 3.8 – 7.6 cm/yr) between the different cases. Velocities are approximately constant in the shallowest layers, however, below the lithosphere a (local) maximum

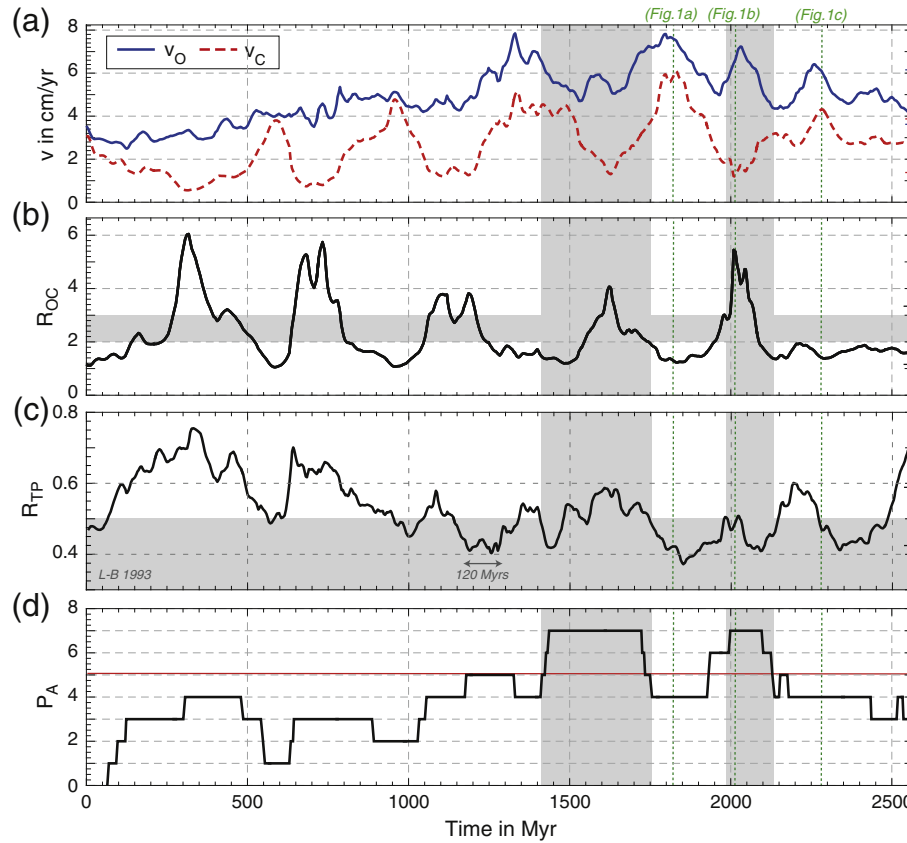


Fig. 3. Time evolution of case M8: (a) rms-surface velocity (continental average: v_C , oceanic average: v_O). Dots and error bars denote means and standard deviations. (b) Ratio of oceanic and continental plate speed R_{OC} , the horizontal shaded region indicates a plausible range for Earth's surface motions since 230 Ma (Zahirovic et al., 2015). (c) Toroidal-poloidal partitioning of surface motions R_{TP} . The shaded region denotes the range inferred for Earth since 120 Ma (Lithgow-Bertelloni et al., 1993, excluding net rotation). (d) Number of assembled continent pairs P_A (see text). The horizontal line highlights $P_A = N_C - 1 = 5$. In all panels, shaded vertical columns denote when all continents are assembled. Vertical dotted lines indicate when the snapshots in Fig. 1 are taken.

may be observed, which is caused by the applied viscosity reduction within the asthenosphere. However, the strength of this effect varies between the models, which points to more or less pronounced asthenospheric viscosity reduction underneath the plates (see also Fig. 4a). At greater depth, velocities quickly decrease to a significantly

reduced lower mantle velocity. Predicted surface and upper mantle velocities essentially correlate with upper mantle viscosity.

Moreover, the viscosity contrast $\Delta\eta_R$ exerts the most important control on continental drift speed v_C and the partitioning factor R_{OC} , since larger $\Delta\eta_R$ directly reduces upper mantle viscosity in our

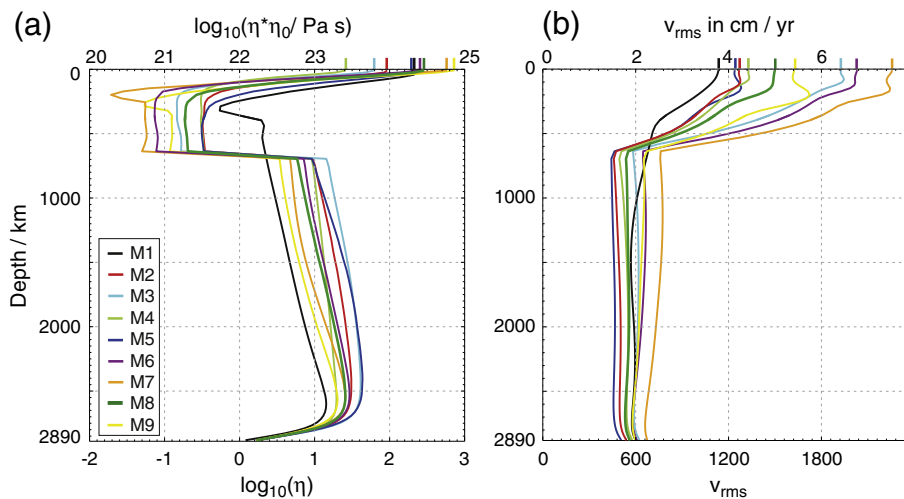


Fig. 4. Time-averaged radial profiles of (a) viscosity η and (b) rms velocity v_{rms} . For the lateral averaging of η the median is used instead of the mean to avoid dominance of the very viscous cratons. The vertical bars on top of the panels highlight the surface values. See Appendix A for the scaling between non-dimensional and dimensional values.

model. This is the anchoring viscosity for the thick continental roots and may thus determine the magnitude of the resistive drag at their base. Consequently, increasing $\Delta\eta_R$ leads to faster continental drift (Fig. 5a) and weaker oceanic-continental speed partitioning (Fig. 5b). In addition, toroidal flow may be less important (R_{TP} decreases with increasing $\Delta\eta_R$, Fig. 5c), which may be linked to the smaller lateral viscosity variations across the surface (see Fig. 2b).

Similar effects, but with somewhat different magnitudes, are observed upon an increase of the activation energy E_A . With our setup, increased values of E_A effectively lead to similar upper mantle viscosities and average surface plate velocities (Fig. 4). However, they also leads to a stiffer and thicker lithosphere. As we will demonstrate below, this supports larger plates and promotes longer-wavelength flow in which continents tend to be more clustered. Plates with such large continental assemblies tend to move slower, such that a decrease in v_C , thus, an increase in R_{OC} is observed with larger E_A . Because the activation energy determines the sensitivity of viscosity to temperature and the strength of lateral viscosity variation, the observed strong increase in the toroidal-poloidal partitioning at the surface is somewhat expected (Fig. 5c).

The lithosphere's resistance to plastic yielding is determined by the yield strength (here specifically σ_0). Increasing σ_0 allows larger plates to form. However, the mantle underneath such large plates tends to be hotter, such that upper mantle viscosity is reduced, also because more asthenospheric viscosity reduction occurs and a thicker and more wide-spread weak asthenosphere is observed. Consequently, surface plate motions are generally increased (Fig. 4b). However, this trend does not hold for continental plate speeds for which no consistent variation is observed across the range of σ_0

tested here (Fig. 5d). Again, we argue that larger plates are an expression of longer wavelength flow, which facilitates the assembly of continents (see below) and thus reduces their average drifting speed. This may balance the enhancing effect of reduced upper mantle viscosity and explain the approximately constant continental drift speed for different σ_0 . However, continental clustering has evidently less effect on oceanic plates, which dominate the global average in Fig. 4b, thus, continent-ocean speed ratios (R_{OC}) may still increase with increasing σ_0 (Fig. 5e). Finally, changes in σ_0 seem to cause smaller variation in R_{TP} than changes in E_A or in $\Delta\eta_R$ (compare panels c and f in Fig. 5). This is consistent with the seemingly less pronounced differences in the strength of lateral viscosity variation (Fig. 2b). However, the origin of this observation remains to be further evaluated.

3.4. Rheological controls on continental configuration evolution

Finally, we compare the evolution of continental configuration (via P_A) for the different cases (Fig. 6). Due to the dispersed initial configuration is $P_A = 0$ at $t = 0$ for all cases, but the first collisions occur soon after the onset of continental drift (note again that the first 500 Myr are excluded from any temporal averaging).

Afterwards, a totally dispersed configuration cannot be observed again. Case M4 is an exception, because it features the weakest lithosphere and the smallest viscosity contrast between lithosphere and upper mantle (Fig. 4a), such that large plates are not supported. Consequently, the characteristic plate size becomes smaller than the mean free path between the six continents and continental assembly is very inefficient. All other cases always feature at least a moderate

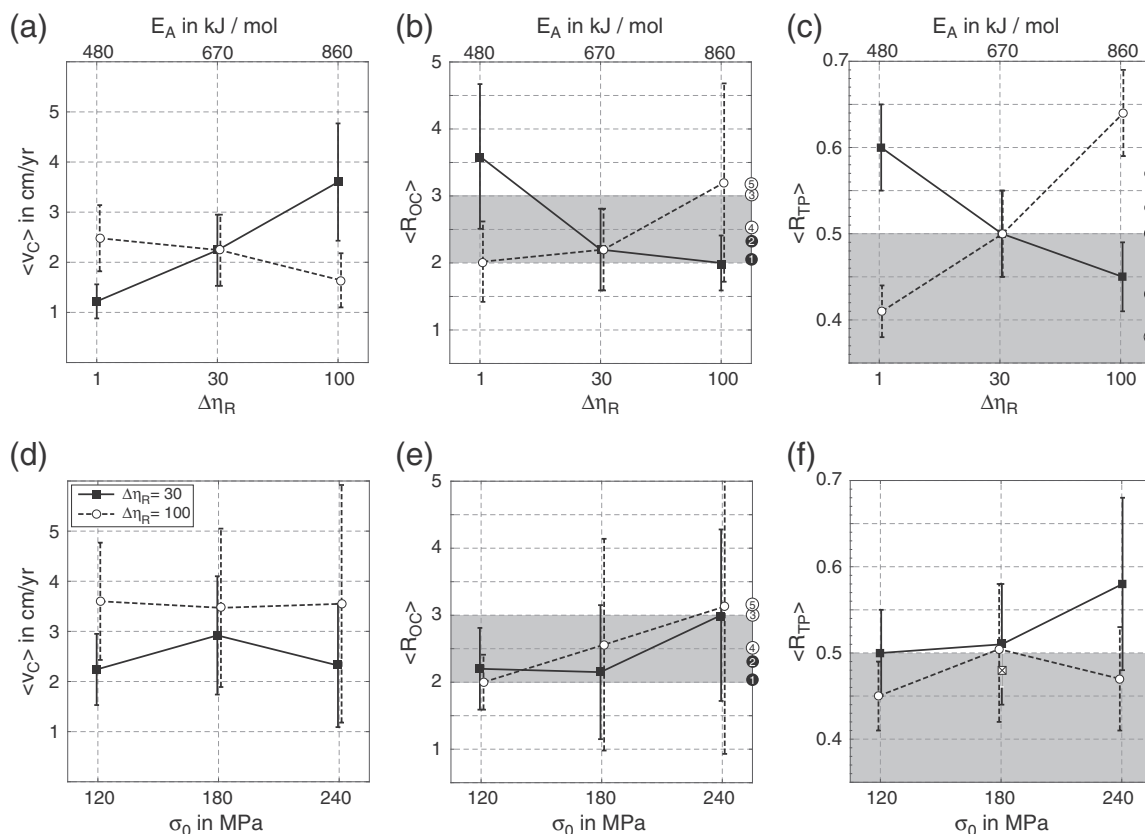


Fig. 5. Control of rheological parameters on time-averaged ($\langle \cdot \rangle$) (a) v_C , (b) R_{OC} , and (c) R_{TP} . Bold: cases with varying $\Delta\eta_R$ (using lower x-axis); dashed: cases with varying E_A (upper x-axis). Squares, respectively, circles denote mean values, error bars denote standard deviations. (d)–(f) are identical to (a)–(c), but for cases with varying σ_0 using $\Delta\eta_R = 30$ (solid) or $\Delta\eta_R = 100$ (dashed). Numbered circles on the y-axes denote present-day estimates as given in Becker (2006): (1) GSRM model (Kreemer et al., 2003), (2) NUVEL-1 model (DeMets et al., 1990), (3)–(5) free-slip cases 3–5 of Becker (2006). Only (1) and (2) are employing a no lithospheric net rotation reference frame as used here. Shaded regions are defined as in Fig. 3. The white crossed square in panel (f) denotes case M8nc without continents.

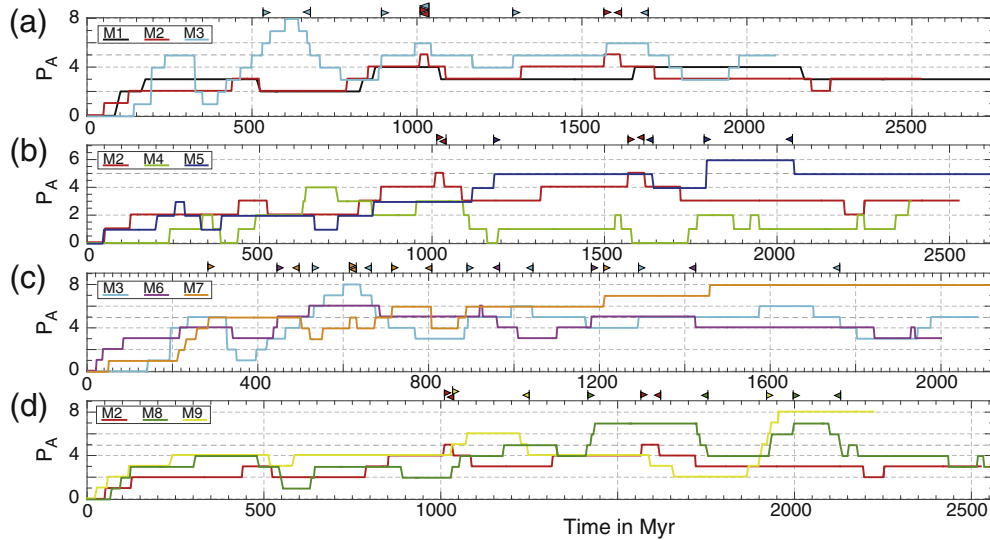


Fig. 6. Evolution of continental configuration proxy P_A for cases with varying (a) $\Delta\eta_R$, (b) E_A , (c) σ_0 (using $\Delta\eta_R = 100$), and (d) σ_0 (using $\Delta\eta_R = 30$). Left-/right-pointing flags indicate the begin/end of a period of complete aggregation (i.e. any assembly of all six continents).

degree of continental clustering throughout their evolution, similar to modern Earth since the break-up of Pangea. The other configuration end-member, i.e. long periods of very compact clustering ($P_A = 7-8$) is also observed, e.g. in case M7, which features a compact supercontinent with a lifetime of 1 Gyr or more (Fig. 6c). Such compact clusters are difficult to disperse once formed (see Rolf et al., 2014) and mainly occur in the cases with the highest yield stress.

However, an evolution representative of Earth’s tectonics should fall in between these two end-members given the evidence of both continental collisions and break-ups in the geological record. This requires phases with moderate degrees of connectivity (P_A) interrupted (at least once) by a phase of high connectivity indicating supercontinent configuration, such as in the reference case M8 (Figs. 1 and 6d).

A trend towards higher connectivity for increased E_A and σ_0 is present, but its robustness is difficult to assess with the available simulations, which would ideally cover longer time spans and a wider range of the input parameters. Instead, we investigate here an effective proxy, the mean characteristic spherical harmonic degree L_C , which is computed after decomposing the obtained flow solutions (temperature field) into spherical harmonics L_n (of degree n). L_C is then the average over the L_n weighted by their relative power. We note that the measure L_C is sensitive to perturbations from higher L

and thus does not reveal the dominant degree (the L_n with strongest power). This is typically either L_1 or L_2 (occasionally L_3), which makes it difficult to use the dominant degree to highlight differences between the cases.

Following this approach, we obtain nine different values for L_C which we compare to the time-averaged continental configuration proxy $\langle P_A \rangle$. This reveals a clear relation in which the continents are on average less assembled to each other (smaller $\langle P_A \rangle$) for increasing L_C (decreasing wavelength, Fig. 7a). This relation implies that only those cases (i.e. viscosity profiles) that allow for sufficient shorter-wavelength contributions in the generally long-wavelength flow are prone to episodic clustering and dispersal of continents, while solutions in which the longest wavelength components are too dominant and stable tend to generate too long-living compact supercontinents.

This analysis concerns only time-averaged values of P_A , but a model representative of Earth must feature ongoing collisions and break-ups, thus, sufficient temporal variation in P_A . As a test, we analysed the standard deviation of $\langle P_A \rangle$ (Fig. 7b). Indeed, cases with similar mean feature different temporal variation (compare e.g. cases M6 and M8). However, this may be affected by the preset number of six continents here and the limited integration time (given

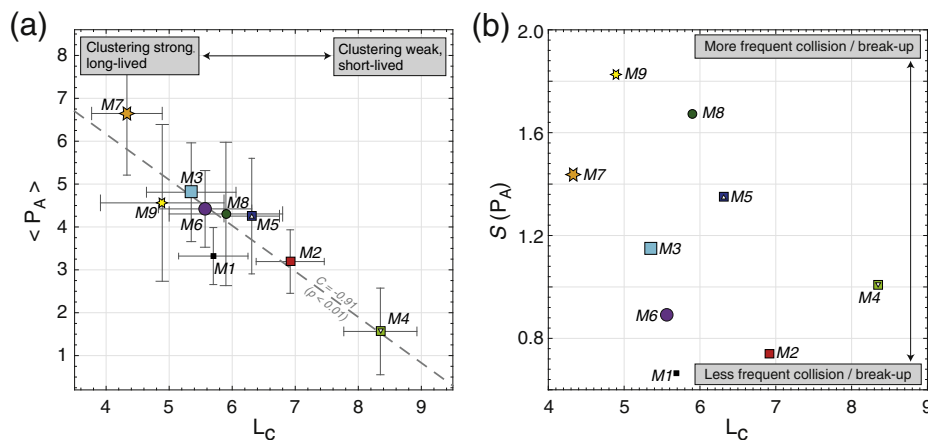


Fig. 7. Continental configuration analysis. (a) Time-averaged $\langle P_A \rangle$ versus characteristic spherical harmonic degree L_C (see text). The dashed grey line is a least-squares fit (C : correlation coefficient, $1-p$: confidence level). (b) Standard deviation $S(P_A)$. Size and shape of symbols are defined as in Fig. 2a.

the long timescales of continental evolution), such that future refinement is certainly necessary in order to increase the significance of this measure.

4. Discussion

We have presented a set of numerical calculations that model Earth's global coupled plate-mantle system including continents. In contrast to other recent efforts to model this time-evolving system (e.g. Zhang et al., 2012; Rudolph and Zhong, 2014; Hassan et al., 2016), we have not imposed kinematic surface constraints that force the system to evolve according to these constraints. While also not completely free of impositions (e.g. the prescribed continent geometry), our approach thus provides a generic view on plate dynamics independent of tectonic reconstructions. It is thus noteworthy that our models reproduce important features of Earth's tectonics, such as the localisation of deformation into narrow plate boundaries that fragment the surface into a heterogeneous network of large and small plates (Morra et al., 2012; Mallard et al., 2016) and episodic collisions and dispersal of continents.

Most of our models are dominated by long-wavelength flow (spherical harmonic degrees L_1 and L_2 , rarely L_3) as expected since they feature several ingredients to promote this style of convection, including continents (Grigné et al., 2007), a low-viscosity asthenosphere (Höink and Lenardic, 2008) as well as high degrees of internal heating combined with a strong lithosphere (McNamara and Zhong, 2005a), and a viscosity jump at 660 km depth (Bunge et al., 1996; Tackley, 1996). Zhong et al. (2007) proposed that mantle flow structure may alternate between L_1 and L_2 dominance in the course of a supercontinent cycle: L_2 dominates after mantle flow reorganisation following the formation of a supercontinent and is maintained until after its break-up before its fragments may start to assemble into a new supercontinent. In contrast, continuous L_2 dominance may be promoted by long-term stability of antipodal large-scale thermochemical structures in the deep mantle as strongly suggested by the reconstructed locations of Earth's large igneous provinces (e.g. Torsvik et al., 2008). This may imply that the characteristic wavelengths of surface tectonics and deep mantle structure are somewhat decoupled. This is consistent with recent 2D convection modelling featuring both continental drift and deep compositional heterogeneity, which does not suggest a spatial correlation between supercontinents and dense compositional provinces (Trim and Lowman, 2016). However, no self-consistent 3D dynamic model has addressed this issue yet and our presented model also does not include deep thermochemical anomalies.

Besides that, the wavelength of mantle flow and its generating viscosity structure are important for whether the model evolutions of continental configuration appear Earth-like or not. In our cases where the longest wavelength components are too dominant and stable, we observe the formation of very compact supercontinents that persist over long timescales (Figs. 6, 7). The resulting time scales of supercontinent stability are rather long for Earth's history, at least if the episodic peaks in the zircon age distributions, separated by ~700–800 Myr (Condie and Aster, 2010), are linked to periods of enhanced continental collisions, i.e. supercontinent formation. This behaviour is most pronounced in cases with high yield strength (M7, M9), i.e. with a higher resistance to lithospheric failure, the formation of plate boundaries and continental break-up (see Rolf et al., 2014).

On the other hand, models with strong short-wavelength contributions complicate the aggregation of large continental clusters, or these have only very short lifetimes. This is preferentially observed if the viscosity contrast between lithosphere and underlying mantle is comparably small ($< \sim 10^{2.5}$, cases M4, M2, Figs. 4a and 6), similar to inferences from models without plastic failure in the lithosphere and continents (McNamara and Zhong, 2005a). On Earth, the existence

of Pangea is well-documented; its exact lifetime is more difficult to infer, but 100 Myr or more seem reasonable (e.g. Stampfli et al., 2013). Moreover, a model representative of Earth should be capable of generating large oceanic plates like the Pacific. Both features are difficult to achieve in those model cases.

A more detailed distinction of cases purely based on the analysis of continental configurations is difficult due to the limited number of calculations, the simplicity of our diagnostic (P_A), and the general permissiveness of this constraint. We have thus also used the ocean-continent speed ratio R_{OC} of plate motions (Figs. 3b, 5) and their toroidal-poloidal partitioning R_{TP} (Figs. 3c, 5) to further assess which model may be most representative for Earth's tectonic evolution.

The inclusion of strong continents generally seems to increase the proportion of toroidal flow in plate motions (Fig. 5f) since they increase the lateral rheological contrast in the lithosphere (see e.g. Wen and Anderson, 1997; Zhong, 2001). However, even without continents significant toroidal motion is generated, such that the dominant source of this type of motion must be related to the plate boundary network and the associated lateral viscosity variations (plate interior/boundary contrast, strength of upper mantle slabs).

Our computed time-averaged R_{TP} values are comparable to those from geodynamic models of the present-day mantle with temperature- and strain rate-dependent rheology (Becker, 2006), although on the high end. It should be noted that the computations of Becker (2006) include net rotation, which is essentially L_1 toroidal motion (Zhong, 2001) and excluded from our solutions here. Our values may thus be more appropriately compared to estimates from a reference frame without net rotation. Becker (2006) reports $R_{TP} = 0.53$, respectively, 0.57 for the plate models of DeMets et al. (1990) and Kreemer et al. (2003). Our case M5 with the strongest lateral viscosity variations generates too much toroidal flow compared to these values (Table 2) and may thus not be the best representative model of Earth.

Regarding time-dependence, Lithgow-Bertelloni et al. (1993) report $R_{TP} \sim 0.25$ – 0.50 for Earth's plate motions since 120 Ma, excluding net rotation. Most cases meet this inferred range throughout large portions of the evolution and generate matching R_{TP} values for time spans of 100 Myr or longer (see Fig. 3c). However, the smaller values of this range, $R_{TP} < 0.4$, are rarely observed in our models, even without continents present. Possibly, this is caused by our simplified parametrisation of rheology. For instance, we do not consider non-linear power-law rheology in the upper mantle, which may help to reduce the computed R_{TP} (Becker, 2006).

All presented cases feature slower motion of continental than oceanic plates ($R_{OC} > 1$) on average, but also throughout the entire evolution, in line with Earth's well-established present-day characteristic (Forsyth and Uyeda, 1975) that has probably also persisted throughout Earth's tectonic evolution (e.g. Zhirovic et al., 2015; Matthews et al., 2016). More specifically, geodynamic models of present-day mantle flow predict $2.5 \leq R_{OC} \leq 3.2$ if employing temperature (and optionally strain rate) dependent viscosity (Becker, 2006), including net rotation though. For tectonic models without net rotation (DeMets et al., 1990; Kreemer et al., 2003), however, R_{TP} may be somewhat lower, 2.1–2.3 (see Becker, 2006). If the latter values are taken as a more appropriate reference for our model, several of our cases overestimate R_{OC} either because upper mantle viscosity (thus, the resistive continental drag) is too high (M1) or because continental clustering is very strong (e.g. M7). The latter may lead to larger area-integrated tractions at the continental base and slow down continental drift (Phillips and Bunge, 2007).

We emphasise that the diagnostic R_{OC} may vary strongly with time, likely in response to changes in continental configuration (Fig. 3b, d). Zhirovic et al. (2015) investigated the partitioning of oceanic and continental plate speeds in their tectonic reconstruction since 230 Ma and suggest that the rms speed of continental plates is typically 2–3× lower than the global one, however, this does

include net rotations. Significant temporal variation in R_{OC} is also evident in their reconstructed speeds, e.g. $R_{OC} \rightarrow 1$ during 60–50 Ma when the North American and the Indian continent moved very fast. However, our models suggest that the largest-amplitude variations occur on timescales of several 100 Myr; thus, they may not be captured by this reconstruction of only the last 230 Ma. Recently, Matthews et al. (2016) suggested that R_{OC} has been almost exclusively >1 since 410 Ma. However, their proposed global decrease of plate motions between 350 Ma and 250 Ma suggests an increase in R_{OC} during this period involving the assembly of Pangea. In contrast, our models indicate that R_{OC} may increase in such conditions since continental plates slow down more than oceanic plates (Fig. 3). A more detailed comparison between our models and long-term reconstructions (Domeier and Torsvik, 2014; Matthews et al., 2016) is thus of future interest.

4.1. Viscosity profile generating the most Earth-like tectonic evolution

The differing ability of our models to match Earth-like characteristics arises from variations in rheological parameters. This may thus be used to infer a suitable mantle viscosity structure that is able to generate an Earth-like tectonic evolution. Using the above considerations on P_A , R_{TP} , and R_{OC} , model M8 seems to be the best representation of Earth, although these constraints arguably include some permissiveness.

Specifically, the inferred viscosity profile features an average upper mantle viscosity of $\eta_{um} \sim 2 \times 10^{21}$ Pa s (Fig. 8). In comparison, a postglacial rebound estimate may be $\eta_{um} \sim 4 \times 10^{20}$ Pa s (Mitrovica and Forte, 2004). Such a value is only approached by model M7 (see Fig. 4), which however tends to generate too strong continental clustering (Fig. 6). Because our applied Rayleigh number is reduced compared to Earth's mantle, plates are somewhat thicker and sinking slabs more negatively buoyant. A larger η_{um} should counteract this effect, such that the balance of tectonic forces is still feasible for generating an Earth-like evolution of surface kinematics. This means that we are mostly able to infer relative variations rather than absolute viscosity values.

In this context, η_{um} is $\sim 10^3 \times$ lower than the viscosity of oceanic plates, which is sufficient to promote very long wavelength flow in the absence of plastic yielding (e.g. McNamara and Zhong, 2005a). Evidently, the cratonic portion of the lithosphere features much higher viscosities than the underlying mantle that are necessary to ensure long-term stability of the cratons (Lenardic et al., 2003; Yoshida, 2012). While we do not deem these values as necessarily realistic, we note that Earth's cratons are likely much more viscous than other lithospheric material because of relative dehydration (e.g. Karato, 2010).

Lower mantle viscosity ranges from $\sim 6 \times 10^{22}$ Pa s just below the transition zone to $\sim 2.5 \times 10^{23}$ Pa s at ~ 2500 km depth. The relatively flat lower mantle profile is in line with inferences from seismic tomography on slab sinking rates (Cizkova et al., 2012). Again, absolute viscosities are on the upper end of estimates (e.g. Mitrovica and Forte, 2004; Steinberger and Calderwood, 2006) because of the somewhat reduced Rayleigh number applied in the model. We also note that with our simplified rheological model, the slight viscosity increase in the lower mantle does not arise from a depth-dependence of mineralogical or thermodynamic parameters (cf. Steinberger and Calderwood, 2006), but from a gradual decrease of superadiabatic temperature, which is typically maximum below the lithosphere in our mostly internally heated models (excluding the bottom ~ 200 km).

We further emphasise that the upper-lower mantle viscosity jump that dominates the total viscosity increase with depth is prescribed: in case M8, $\Delta\eta_R = 30$. This choice is based on constraints derived from Earth's long-wavelength geoid (e.g. Richards and Hager, 1984; Hager et al., 1985), which only deal with radial viscosity variations. The presence of lateral variations may require

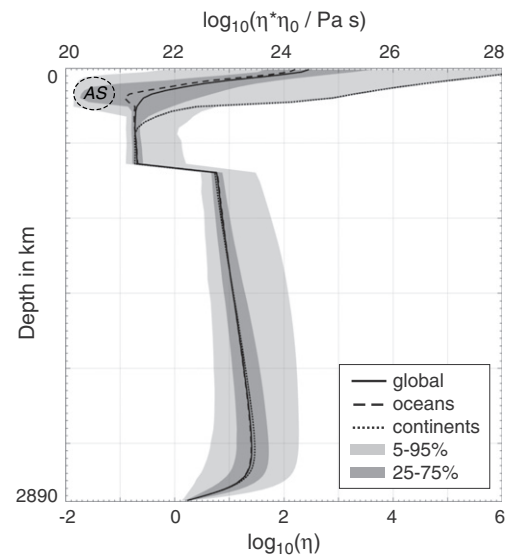


Fig. 8. Time-averaged viscosity profile of case M8 (bold), also partitioned into suboceanic (dashed) and subcontinental domains (dotted). The dark (light) shaded area is bounded by the 25% (5%) and 75% (95%) quantiles. The lateral averaging employs the median as described in Fig. 4a. The approximate depth extend and viscosity range of the parametrised low-viscosity asthenosphere (see main text and Fig. 1) is indicated by the dashed ellipse (AS).

a stronger viscosity increase with depth in order to match regional subduction zone characteristics (e.g. Moresi and Gurnis, 1996; Billen et al., 2003). This has not been taken into account in our global model, although lateral viscosity variations are evidently present across the entire mantle depth range (Figs. 1, 8). Below 300–400 km, their strength is typically ~ 1 – 1.5 orders of magnitude if accounting for the whole range of spatial scales (Fig. 8), but we have not evaluated their long-wavelength variation, which may be smaller. At shallower depth, however, lateral variations are substantially stronger due to the presence of the continental keels and also because of the (non-global, see below) asthenosphere in which the lowest viscosities, here down to $\eta_{AS} \sim 1 \times 10^{20}$ Pa s, are observed.

This asthenospheric viscosity is above the estimates from high-resolution models of instantaneous mantle flow that match present-day plate motions (10^{18} – 10^{19} Pa s, Stadler et al., 2010) and from analysis of postseismic deformation in the Indian ocean (5×10^{17} – 10^{19} Pa s, Hu et al., 2016). One possible explanation for that may be the fixed viscosity reduction factor applied in the asthenosphere ($\Delta\eta_{AS} = 0.1$). This contrast may be significantly stronger depending on water content (see e.g. Masuti et al., 2016) and the resulting lower asthenospheric viscosities likely affect the dynamics on the scale of a subduction zone. Globally, however, they may affect the magnitude of shear tractions at the base of the lithosphere only little compared to the presence of continental keels (e.g. Conrad and Lithgow-Bertelloni, 2006). Thus, plate-mantle coupling and global surface kinematics may not depend strongly on the actual asthenospheric viscosity as long as it is significantly reduced compared to the underlying mantle.

More important may be the lateral extend of the asthenosphere, in particular if it underlies the continental roots, which strongly impacts on the coupling of mantle and lithosphere (Zhong, 2001; Conrad and Lithgow-Bertelloni, 2006). Recently, Yuan and Romanowicz (2010) suggested an asthenospheric layer underneath the North American craton based on seismic anisotropy analysis. Moreover, van Summeren et al. (2012) favour a global over a regional asthenosphere based on matching present-day plate motions. In case M8 (and the presented calculations in general), however, the asthenospheric layer is limited

to suboceanic lithosphere (see e.g. Fig. 1). Below the cratons, viscosity reduction associated with partial melting in the parameterised asthenosphere is only observed in small patchy regions in the cases with highest yield stress (M7, M9), which feature the highest sublithospheric temperatures. However, their extent is small and they are not temporally persisting. Nevertheless, the best-fitting presented models are still capable of generating continent–ocean plate speed ratios (R_{OC}), toroidal–poloidal partitioning (R_{TP}), and continental configuration evolutions in line with Earth’s tectonic evolution. This may imply that they indeed feature an appropriate balance of resisting and driving forces of plate motions. If a global extent of the asthenosphere is not necessary to generate such first-order observations, this would have implications for the partitioning of slab-related plate driving forces, i.e. slab suction and slab pull, and its temporal evolution (e.g. Conrad and Lithgow-Bertelloni, 2002, 2004). However, extension and further refinement of the considered constraints as well as improvements in our model formulation are required (see Section 4.2) before such issues can be addressed thoroughly.

4.2. Model limitations and future improvements

Our model is an advance from previous attempts to jointly simulate time-dependent global mantle flow, plate-like behaviour and continental assembly and dispersal in a dynamically consistent manner. Nevertheless, it should be further improved in future as already discussed above. Including compressibility may influence mantle flow wavelength (e.g. Tackley et al., 1994) and increased convective vigour may impact the quality of plate-like behaviour (Stein et al., 2004; Foley and Becker, 2009; van Heck, 2011) and reduce characteristic lithospheric thickness, which could affect the tectonic force balance. Moreover, phase transitions may modify the dynamics of sinking slabs, e.g. by leading to stagnation at some mid-mantle depth (e.g. Christensen and Yuen, 1984; King et al., 2015), which may feed back on the magnitude of slab pull and suction forces (Conrad and Lithgow-Bertelloni, 2002, 2004).

The style of surface tectonics may also depend on the partitioning of basal and internal heating. Here, we employed high degrees of internal heating ($\sim 85\text{--}90\%$), since this - in combination with a rheologically strong surface boundary layer - favours the generation of long-wavelength flow (McNamara and Zhong, 2005a). Based on a similar model as presented here (but e.g. $\Delta\eta_R = 1$), Coltice et al. (2013) suggested that such weak basal heating has only a small effect on surface velocities and seafloor spreading rates. If basal heating dominates the heat budget though, localisation of deformation in the lithosphere and thus plate-like behaviour may be more difficult to achieve, at least in the absence of continents (e.g. Foley and Becker, 2009). The relative contribution of basal heating to the heat budget of Earth’s mantle is not yet well constrained, but may be $\sim 30\%$ (e.g. Leng and Zhong, 2009), in particular if the core thermal conductivity is very high (Pozzo et al., 2012). 30% basal heating may be sufficient to generate strong plumes that can perturb the paths of drifting continents and complicate their assembly (Phillips and Bunge, 2007). However, Earth displays all of the above ingredients: plate-like behaviour, (strong) mantle plumes and continental assembly. It will thus be important to further constrain the amount of basal heating in the mantle and systematically investigate its role in the resulting surface tectonic history.

Finally, and perhaps most important for our interest, is the problem that our models display too symmetric downwellings compared to Earth’s single-sided subduction, although including continents partly improves this. The artificial subduction symmetry may in fact not have a strong effect on slab sinking rates (Capitanio et al., 2007), but it modifies the partitioning of slab-related plate driving forces (see Conrad and Lithgow-Bertelloni, 2002, 2004) and the torque around plates. This impacts the motion and shape of trenches (e.g. Crameri and Tackley, 2014), the speed partitioning of

subducting and non-subducting plates (Conrad and Lithgow-Bertelloni, 2004; van Summeren et al., 2012) and possibly the generation of toroidal flow (e.g. Alisc et al., 2012) as well as the way how continents assemble and disperse. Global mantle flow models with more realistic subduction behaviour have been proposed (e.g. Stadler et al., 2010). However, global time-dependent models featuring single-sided subduction that develops self-consistently have only recently been developed (Crameri et al., 2012; Crameri and Tackley, 2014) and the implementation of continents into such models remains an important future task.

5. Conclusions

We have conducted models of 3D spherical mantle convection with self-consistent plate-like behaviour and continental drift. The goals of our study have been (i) to assess the role of mantle and lithosphere rheology in the evolution of continental drift and the characteristics of surface plate motions, and (ii) to test the idea if Earth’s peculiar continental drift history with episodic clustering and dispersal may provide additional constraints on the effective mantle viscosity profile. The following remarks summarise our main results:

1. Continental configuration evolution is fundamentally determined by the wavelength of mantle flow and thus, intrinsically, by mantle viscosity structure. If the lithosphere is too weak (less than $\sim 10^{2.5} \times$ the upper mantle viscosity), it can be broken more easily by convective stresses and shorter-wavelength components contribute more strongly to the flow. The result is a network of too many and too small plates in which continental collisions are less likely to occur. Thus, clustering to form supercontinents does not happen or is very short-lived. Such behaviour is favoured by a low yield strength of the lithosphere and/or relatively weak temperature dependence of viscosity. In the opposite case (very stable longest-wavelength flow), large oceanic plates can form. However, continents tend to form compact clusters, which are difficult to break-up and disperse over timescales relevant for Earth’s continental evolution. This behaviour is strongly favoured by a high yield strength of the lithosphere.
2. Constraints on continental drift histories are rather permissive, but can be supported by characteristic measures of plate motions (oceanic–continental plate speed ratio, toroidal–poloidal partitioning). Then, our models generate the most Earth-like tectonic evolution in terms of continental drift history with episodic collision and dispersal events when employing an intermediately high lithospheric strength (~ 180 MPa) and a viscosity contrast of ~ 30 at the upper–lower mantle transition. Oceanic plates are then $\sim 10^3 \times$ more viscous than the underlying upper mantle and viscosity increases by a factor of 100–200 from the uppermost mantle (excluding the asthenosphere) to the lowermost mantle. This structure causes continents to move $\sim 2.2 \times$ slower than oceanic plates on average and generates plate motions, which have toroidal components as strong as $\sim 50\%$ of the poloidal components, in line with estimates from kinematic reconstructions.
3. No globally extending low-viscosity asthenosphere is required to match the continent–ocean plate speed ratios inferred for present-day and from tectonic reconstructions. In this case, the asthenosphere is limited to major regions below oceanic plates. Its extent depends on the size of the tectonic plates (which affects sublithospheric temperature), but does not involve the region below the thickest continental roots, which suggests a stronger coupling of plates and underlying mantle.
4. The plate speed ratio of continental and oceanic plates may vary strongly with time, importantly on timescales of several 100 Myr. The partitioning may be maximum following phases

of enhanced continental assembly and minimum for generally dispersing continents. These timescales exceed conventional reconstructions, but may become a testable feature once reconstructions from the Paleozoic until present will have been established.

Acknowledgments

TR receives funding from the Norwegian Research Council through a Centre of Excellence grant to the Centre for Earth Evolution and Dynamics (CEED, project number 223272). Computations have been performed on Stallo, a Notur facility at the University of Tromsø, under project code nn9283 and on Monte Rosa, a facility of the Swiss National Supercomputing Centre (CSCS), under project ID s272. The authors thank M. Gurnis and T. Becker for their constructive reviews and N. Coltice for his comments on an earlier version of the manuscript.

Appendix A. Dimensionalisation of results

Non-dimensional input parameters and results have been converted to dimensional numbers. Since model convective vigour and thus convective velocities may be lower than in Earth's mantle, the transit time framework is used, which is based on equalising Earth's mantle transit time with its numerical model analogue. Earth's mantle transit time τ_E is the time needed to cross the mantle with a characteristic velocity, here the present-day rms surface velocity; the reconstruction of Seton et al. (2012) gives $\sim 4.6\text{cmyr}^{-1}$, thus, $\tau_E \sim 63\text{Myr}$. Note that this choice is rather arbitrary and not necessarily a characteristic of Earth's long-term evolution.

The model analogue τ employs the time-averaged non-dimensional rms surface velocity of the reference case M8, which leads to $\tau \sim 7.276 \times 10^{-4}$. The factor τ/τ_E connects model and Earth timescales and relates dimensional and non-dimensional properties as follows: (time) $t_{(\text{Myr})} = t\tau_E/\tau$, (velocity) $v_{(\text{cm/yr})} = vD_0\tau/\tau_E$, (temperature) $T_{(\text{K})} = T_S + T\Delta T$, (viscosity) $\eta_{(\text{Pa s})} = \eta_0\eta$, (depth) $d_{(\text{m})} = D_0d$, (yield stress) $\sigma_{(\text{Pa})} = \sigma\eta_0\tau/\tau_E$, (yield stress gradient) $\sigma'_{(\text{Pa/m})} = \sigma'\eta_0\tau/D_0\tau_E$, (activation energy) $E_{A_{(\text{J/mol})}} = E_A R_g \Delta T$ with R_g being the gas constant, and (internal heating rate) $H_{(\text{W/kg})} = Hk_0\Delta T/\kappa_0\rho_0\tau_E$.

References

- Alisic, L., Gurnis, M., Stadler, G., Burstedde, C., Ghattas, O., 2012. Multi-scale dynamics and rheology of mantle flow with plates. *J. Geophys. Res.* 117, B10402.
- Becker, T., 2006. On the effect of temperature and strain-rate dependent viscosity on global mantle flow, net rotation and plate-driving forces. *Geophys. J. Int.* 167, 943–957.
- Bercovici, D., Ricard, Y., Richards, M., 2000. The history and dynamics of global plate motions. *Am. Geophys. Union* 121, 5–46. Chapter: The Relation Between Mantle Dynamics and Plate Tectonics: A Primer.
- Billen, M., Gurnis, M., Simons, M., 2003. Multiscale dynamics of the Tonga-Kermadec subduction zone. *Geophys. J. Int.* 153, 359–388.
- Bird, P., 2003. An updated digital model of plate boundaries. *Geochem. Geophys. Geosyst.* 4, 1027.
- Brandl, P., Regelous, M., Beler, C., Haase, K., 2013. High mantle temperatures following rifting caused by continental insulation. *Nature Geosci.* 6, 391–394.
- Bull, A., Domeier, M., Torsvik, T., 2014. The effect of plate motion history on the longevity of deep mantle heterogeneities. *Earth Planet. Sci. Lett.* 401, 172–182.
- Bunge, H., Richards, M., Baumgardner, J., 1996. Effect of depth-dependent viscosity on the planform of mantle convection. *Nature* 379, 436–438.
- Capitanio, F., Morra, G., Goes, S., 2007. Dynamic models of downgoing plate-buoyancy driven subduction: subduction motions and energy dissipation. *Earth Planet. Sci. Lett.* 262, 284–297.
- Christensen, U.R., Yuen, D., 1984. The interaction of a subducting lithospheric slab with a chemical or phase boundary. *J. Geophys. Res.* 89, 4389–4402.
- Cizkova, H., van den Berg, A., Spakman, W., Matyska, C., 2012. The viscosity of Earth's lower mantle inferred from sinking speed of subducted lithosphere. *Phys. Earth Planet. Int.* 200–201, 56–62.
- Coltice, N., Bertrand, H., Rey, P., Jourdan, F., Phillips, B., Ricard, Y., 2009. Global warming of the mantle beneath continents back to the Archaean. *Gondwana Res.* 15, 254–266.
- Coltice, N., Rolf, T., Tackley, P., Labrosse, S., 2012. Dynamic causes of the relation between area and age of the ocean floor. *Science* 336, 335–338.
- Coltice, N., Seton, M., Rolf, T., Müller, R., Tackley, P., 2013. Convergence of tectonic reconstructions and mantle convection models for significant fluctuations in seafloor spreading. *Earth Planet. Sci. Lett.* 383, 92–100.
- Condie, K., Aster, R., 2010. Episodic zircon age spectra of orogenic granitoids: the supercontinent connection and continental growth. *Precambrian Res.* 180, 227–236.
- Conrad, C., Lithgow-Bertelloni, C., 2002. How mantle slabs drive plate tectonics. *Science* 298, 207–209.
- Conrad, C., Lithgow-Bertelloni, C., 2004. The temporal evolution of plate driving forces: importance of “slab suction” versus “slab pull” during the Cenozoic. *J. Geophys. Res.* 109, B10477.
- Conrad, C., Lithgow-Bertelloni, C., 2006. Influence of continental roots and asthenosphere on plate-mantle coupling. *Geophys. Res. Lett.* 33, L05312.
- Cramer, F., Tackley, P., 2014. Spontaneous development of arcuate single-sided subduction in global 3-D mantle convection models with a free surface. *J. Geophys. Res.* 119, 5921–5942.
- Cramer, F., Tackley, P., Meilick, I., Gerya, T., Kaus, B., 2012. A free plate surface and weak oceanic crust produce single-sided subduction on Earth. *Geophys. Res. Lett.* 39, L03306.
- DeMets, C., Gordon, R., Argus, D., Stein, S., 1990. Current plate motions. *Geophys. J. Int.* 101, 425–478.
- Doin, M., Fleitout, L., Christensen, U., 1997. Mantle convection and stability of depleted and undepleted continental lithosphere. *J. Geophys. Res.* 102, 2771–2787.
- Domeier, M., Torsvik, T., 2014. Plate tectonics in the late Paleozoic. *Geosci. Frontiers* 5, 303–350.
- Domeier, M., Van der Voo, R., Torsvik, T., 2012. Paleomagnetism and Pangea: the road to reconciliation. *Tectonophysics* 514–517, 14–43.
- Foley, B., Becker, T., 2009. Generation of plate-like behavior and mantle heterogeneity from a spherical, viscoplastic convection model. *Geochem. Geophys. Geosyst.* 10, 2009GC002378.
- Forsyth, D., Uyeda, S., 1975. On the relative importance of the driving forces of plate motion. *Geophys. J. R. Astr. Soc.* 43, 163–200.
- Gordon, R., 1998. The plate tectonic approximation: plate nonrigidity, diffuse plate boundaries, and global plate reconstructions. *Annu. Rev. Earth Planet. Sci.* 26, 615–642.
- Grigné, C., Labrosse, S., Tackley, P., 2007. Convection under a lid of finite conductivity in wide aspect ratio models: effect of continents on the wavelength of mantle flow. *J. Geophys. Res.* 112, B08403.
- Gurnis, M., 1988. Large-scale mantle convection and the aggregation and dispersal of supercontinents. *Nature* 332, 695–699.
- Hager, B., Clayton, R., Richards, M., Comer, R., Dziewonski, A., 1985. Lower mantle heterogeneity, dynamic topography and the geoid. *Nature* 313, 541–545.
- Hassan, R., Müller, R., Gurnis, M., Williams, S., Flament, N., 2016. A rapid burst in hotspot motion through the interaction of tectonics and deep mantle flow. *Nature* 533, 239–244.
- Heron, P., Lowman, J., Stein, C., 2015. Influences on the positioning of mantle plumes following supercontinent formation. *J. Geophys. Res.* 120, 3628–3648.
- Höink, T., Lenardic, A., 2008. Three-dimensional mantle convection simulations with a low-viscosity asthenosphere and the relationship between heat flow and the horizontal length scale of convection. *Geophys. Res. Lett.* 35, L10304.
- Hu, Y., Bürgmann, R., Banerjee, P., Feng, L., Hill, E., Ito, T., Tabei, T., Wang, K., 2016. Asthenosphere rheology inferred from observations of the 2012 Indian Ocean earthquake. *Nature* 538, 368–372.
- Karato, S.-I., 2010. Rheology of the deep upper mantle and its implications for the preservation of the continental roots: a review. *Tectonophysics* 481, 82–98.
- King, S., Frost, D., Rubie, D., 2015. Why cold slabs stagnate in the transition zone. *Geology* 43, 231–234.
- Kreemer, C., Holt, W., Haines, A., 2003. An integrated global model of present-day plate motions and plate boundary deformation. *Geophys. J. Int.* 154, 5–34.
- Lenardic, A., Moresi, L.-N., 1999. Some thoughts on the stability of cratonic lithosphere: effects of buoyancy and viscosity. *J. Geophys. Res.* 104, 12747–12758.
- Lenardic, A., Moresi, L.-N., Mühlhaus, H., 2003. Longevity and stability of cratonic lithosphere: insights from numerical simulations of coupled mantle convection and continental tectonics. *J. Geophys. Res.* 108, ETG 9.
- Leng, W., Zhong, S., 2009. More constraints on internal heating rate of the Earth's mantle from plume observations. *Geophys. Res. Lett.* 36, L02306.
- Lithgow-Bertelloni, C., Richards, M., Ricard, Y., O'Connell, R., Engebretson, D., 1993. Toroidal-poleoidal partitioning of plate motions since 120 Ma. *Geophys. Res. Lett.* 20, 375–378.
- Lowman, J., Gable, C., 1999. Thermal evolution of the mantle following continental aggregation in 3D convection models. *Geophys. Res. Lett.* 26, 2649–2652.
- Mallard, C., Coltice, N., Seton, M., Müller, R., Tackley, P., 2016. Subduction controls the distribution and fragmentation of Earth's tectonic plates. *Nature* 535, 140–143.
- Masuti, S., Barbot, S., Karato, S.-I., Feng, L., Banerjee, P., 2016. Upper-mantle water stratification inferred from observations of the 2012 Indian Ocean earthquake. *Nature* 538, 373–377.
- Matthews, K., Maloney, K., Zahirovic, S., Williams, S., Seton, M., Müller, R., 2016. Global plate boundary evolution and kinematics since the late Paleozoic. *Glob. Planet. Change* 146, 226–250.
- McNamara, A., Zhong, S., 2005a. Degree-one mantle convection: dependence on internal heating and temperature-dependent rheology. *Geophys. Res. Lett.* 32, L01301.

- McNamara, A., Zhong, S., 2005b. Thermochemical structures beneath Africa and the Pacific Ocean. *Nature* 437, 1136–1139.
- Mitrovica, J., Forte, A., 2004. A new inference of mantle viscosity based upon joint inversion of convection and glacial isostatic adjustment data. *Earth Planet. Sci. Lett.* 225, 177–189.
- Moresi, L., Gurnis, M., 1996. Constraints on the lateral strengths of slabs from three-dimensional dynamic flow models. *Earth Planet. Sci. Lett.* 138, 15–28.
- Morra, G., Seton, M., Quevedo, L., Müller, R., 2012. Organization of the tectonic plates in the last 200 Myr. *Earth Planet. Sci. Lett.* 373, 93–101.
- Pearson, D., Parman, S., Nowell, G., 2007. A link between large mantle melting events and continent growth seen in osmium isotopes. *Nature* 449, 203–205.
- Phillips, B., Bunge, H.-P., 2005. Heterogeneity and time dependence in 3D spherical mantle convection models with continental drift. *Earth Planet. Sci. Lett.* 233, 121–135.
- Phillips, B., Bunge, H.-P., 2007. Supercontinent cycles disrupted by strong mantle plumes. *Geology* 35, 847–850.
- Pozzo, M., Davies, C., Gubbins, D., Alfè, D., 2012. Thermal and electrical conductivity of iron at Earth's core conditions. *Nature* 485, 355–358.
- Richards, M., Hager, B., 1984. Geoid Anomalies in a dynamic Earth. *J. Geophys. Res.* 89, 5987–6002.
- Rolf, T., Coltice, N., Tackley, P., 2012. Linking continental drift, plate tectonics and the thermal state of the Earth's mantle. *Earth Planet. Sci. Lett.* 351–352, 134–146.
- Rolf, T., Coltice, N., Tackley, P., 2014. Statistical cyclicity of the supercontinent cycle. *Geophys. Res. Lett.* 41, 2351–2358.
- Rudolph, M., Zhong, S., 2014. History and dynamics of net rotation of the mantle and lithosphere. *Geochem. Geophys. Geosyst.* 15, 3645–3657.
- Seton, M., Müller, R., Zahirovic, S., Gaina, C., Torsvik, T., Shephard, G., Talsma, A., Gurnis, M., Turner, M., Maus, S., Chandler, M., 2012. Global continental and ocean basin reconstructions since 200 Ma. *Earth-Sci. Rev.* 113, 212–270.
- Stadler, G., Gurnis, M., Burstedde, C., Wilcox, L., Alisc, L., Ghattas, O., 2010. The dynamics of plate tectonics and mantle flow: from local to global scales. *Science* 329, 1033–1038.
- Stampfli, G., Hochard, C., Vèrard, C., Wilhem, C., von Raumer, J., 2013. The formation of Pangea. *Tectonophysics* 593, 1–19.
- Stein, C., Schmalz, J., Hansen, U., 2004. The effect of rheological parameters on plate behaviour in a self-consistent model of mantle convection. *Phys. Earth Planet. Int.* 142, 225–255.
- Steinberger, S., Calderwood, A., 2006. Models of large-scale viscous flow in the Earth's mantle with constraints from mineral physics and surface observations. *Geophys. J. Int.* 167, 1461–1481.
- van Summeren, J., Conrad, C., Lithgow-Bertelloni, C., 2012. The importance of slab pull and a global asthenosphere to plate motions. *Geochem. Geophys. Geosyst.* 3, Q0AK03.
- Tackley, P., 1996. On the ability of phase transitions and viscosity layering to induce long wavelength heterogeneity in the mantle. *Geophys. Res. Lett.* 23, 1985–1988.
- Tackley, P., 2000a. The history and dynamics of global plate motions. In: Richards, M., Gordon, R., van der Hilst, R. (Eds.), *Geophysical Monographs*. Chapter: The Quest for Self-consistent Generation of Plate Tectonics in Mantle Convection Models 121. American Geophysical Union., pp. 47–72.
- Tackley, P., 2000b. Self-consistent generation of tectonic plates in time-dependent, three-dimensional mantle convection simulations, 1. Pseudoplastic yielding. *Geochem. Geophys. Geosyst.* 1, 2000GC000036.
- Tackley, P., 2000c. Self-consistent generation of tectonic plates in time-dependent, three-dimensional mantle convection simulations, 2. Strain weakening and asthenosphere. *Geochem. Geophys. Geosyst.* 1, 2000GC000043.
- Tackley, P., 2008. Modelling compressible mantle convection with large viscosity contrasts in a three-dimensional spherical shell using the yin-yang grid. *Phys. Earth Planet. Int.* 171, 7–18.
- Tackley, P., King, S., 2003. Testing the tracer ratio method for modeling active compositional fields in mantle convection simulations. *Geochem. Geophys. Geosyst.* 4, 2001GC00214.
- Tackley, P., Stevenson, D., Glatzmaier, G., Schubert, G., 1994. Effects of multiple phase transitions in a three-dimensional spherical model of convection in Earth's mantle. *J. Geophys. Res.* 99, 15877–15901.
- Torsvik, T., Müller, R., Van der Voo, R., Steinberger, B., Gaina, C., 2008. Global plate motion frames: toward a unified model. *Rev. Geophys.* 46, RG3004.
- Trim, S., Lowman, J., 2016. Interaction between the supercontinent cycle and the evolution of intrinsically dense provinces in the deep mantle. *J. Geophys. Res.* 121, 8941–8969.
- van Heck, H., 2011. Scaling of plate tectonics on terrestrial planets. Ph.D. thesis. ETH Zurich
- van Heck, H., Tackley, P., 2008. Planforms of self-consistently generated plates in 3D spherical geometry. *Geophys. Res. Lett.* 35, L19312.
- Wen, L., Anderson, D., 1997. Present-day plate motion constraint on mantle rheology and convection. *J. Geophys. Res.* 102, 24639–24653.
- Xie, S., Tackley, P., 2004. Evolution of U-Pb and Sm-Nd systems in numerical models of mantle convection and plate tectonics. *J. Geophys. Res.* 109, B11204.
- Yoshida, M., 2008. Mantle convection with longest-wavelength thermal heterogeneity in a 3-D spherical model: degree one or two? *Geophys. Res. Lett.* 35, L23302.
- Yoshida, M., 2012. Dynamic role of the rheological contrast between cratonic and oceanic lithospheres in the longevity of cratonic lithosphere: a three-dimensional numerical study. *Tectonophysics* 532–535, 156–166.
- Yoshida, M., 2013. Mantle temperature under drifting deformable continents during the supercontinent cycle. *Geophys. Res. Lett.* 40, 1–6.
- Yoshida, M., Hamano, Y., 2015. Pangea breakup and northward drift of the Indian subcontinent reproduced by a numerical model of mantle convection. *Sci. Rep.* 5, 8047.
- Yoshida, M., Santosh, M., 2014. Mantle convection modeling of the supercontinent cycle: introversion, extroversion, or a combination? *Geosci. Frontiers* 5, 77–81.
- Yuan, H., Romanowicz, R., 2010. Lithospheric layering in the North American craton. *Nature* 466, 1063–1068.
- Zahirovic, S., Müller, R., Seton, M., Flament, N., 2015. Tectonic speed limits from plate kinematic reconstructions. *Earth Planet. Sci. Lett.* 418, 40–52.
- Zhang, N., Zhong, S., Flowers, R., 2012. Predicting and testing continental vertical motion histories since the Paleozoic. *Earth Planet. Sci. Lett.* 317–318, 426–435.
- Zhang, N., Zhong, S., McNamara, A., 2009. Supercontinent formation from stochastic collision and mantle convection models. *Gondwana Res.* 15, 267–275.
- Zhong, S., 2001. Role of ocean-continent contrast and continental keels on plate motion, net rotation of lithosphere, and the geoid. *J. Geophys. Res.* 106, 703–712.
- Zhong, S., Zhang, N., Li, Z., Roberts, J., 2007. Supercontinent cycles, true polar wander, and very long-wavelength mantle convection. *Earth Planet. Sci. Lett.* 261, 551–564.